Chapter 19
Global Climate Change Impacts on Local Climate and Hydrology

Lutz Breuer, Jean-François Exbrayat, Ina Plesca, Wouter Buytaert, Theresa Ehmann, Thorsten Peters, Edison Timbe, Katja Trachte, and David Windhorst

19.1 Introduction

The significant warming trend forecasted by climate models for the tropical Andes is emphasized with increasing altitudes (Urrutia and Vuille 2009). Based on reanalysis data from the National Centers for Environmental Prediction (NCEP)/ National Center for Atmospheric Research (NCAR) these warming trends are already visible for the grid cell of southern Ecuador, showing a warming trend of +0.22 °C per decade since 1948 (Bendix et al. 2010; see also Fig. 2.4). Contradicting this trend, local measurements at the meteorological station at Estación Científica San Francisco (ECSF) within the Rio San Francisco valley show a significant net cooling ($\tau = -0.045$, $P < 0.0001$, $n = 4{,}532$, Seasonal Mann–Kendall test used for daily temperature series) during 1998–2010 (Fig. 19.1). This cooling trend can be ascribed to an increase in daily temperature ranges ($\tau = 0.124$, $P < 0.0001$, $n = 4{,}532$, Seasonal Mann–Kendall test used for daily temperature series) resulting in a decrease in daily minimum temperatures

L. Breuer (✉) • I. Plesca • T. Ehmann • D. Windhorst
Institute for Landscape Ecology and Resources Management, University of Gießen, Gießen, Germany
e-mail: lutz.breuer@umwelt.uni-giessen.de

J.-F. Exbrayat
Climate Change Research Centre, University of New South Wales, Sydney, Australia

W. Buytaert
Department of Civil and Environmental Engineering, Imperial College London, London, UK

T. Peters
Geographic Institute, University of Erlangen, Erlangen, Germany

E. Timbe
Grupo de Ciencias de la Tierra y del Ambiente, Universidad de Cuenca, Cuenca, Ecuador

K. Trachte
Faculty of Geography, University of Marburg, Marburg, Germany

J. Bendix et al. (eds.), *Ecosystem Services, Biodiversity and Environmental Change in a Tropical Mountain Ecosystem of South Ecuador*, Ecological Studies 221,
DOI 10.1007/978-3-642-38137-9_19,

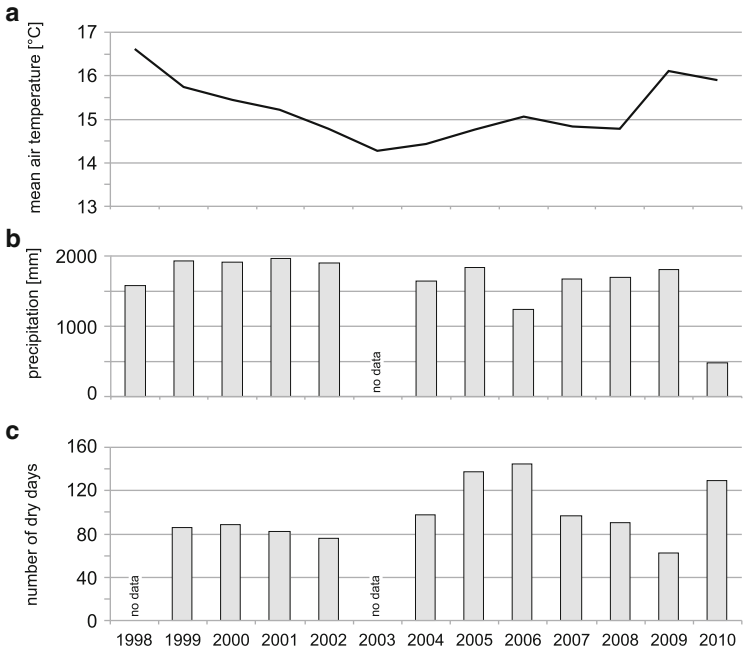

Fig. 19.1 Local climate trends measured during the last 12 years at the ECSF meteorological station (see Fig. 1.2): (**a**) mean annual air temperature, (**b**) precipitation, and (**c**) number of dry days

($\tau = -0.148$, $P < 0.0001$, $n = 4{,}532$) as well as an increase in daily maximum temperatures ($\tau = 0.085$, $P < 0.0001$, $n = 4{,}532$).

In comparison with temperature, projections for changes in precipitation are spatially much less cohesive, with regions of decreased and increased precipitation scattered across the Andean mountain chain (Urrutia and Vuille 2009). Analyses of local precipitation trends show a strong interannual variation (Fig. 19.1) and a clear negative trend during 1998–2010 ($\tau = -0.048$, $P < 0.0001$, $n = 4{,}171$, Seasonal Mann–Kendall test used for daily precipitation series). This can be caused by changes in the intensity and frequency of precipitation events as well as by changes in the number of dry days (see also Fig. 2.4). The latter is probably true for the study region, where a nonsignificant increase in the number of dry days (daily precipitation $= 0$ mm) is observed ($\tau = 0.08$, $P = 0.235$, $n = 154$, Seasonal Mann–Kendall test used for monthly dry day series, Fig. 19.1). This may have more extensive impacts on environmental and human systems than the registered temperature changes.

The question remains how likely future global climate change will impact local climate and hydrology. To investigate these potential effects for the Reserva Biologica San Francisco (RBSF, see Fig. 1.1) we conducted a sensitivity study using simple, statistically downscaled future projections based on General Circulation model (GCM) scenarios for Ecuador and used this dataset to force a set of

hydrological catchment rainfall-runoff models to calculate possible changes of regional discharge.

19.2 Material and Methods

19.2.1 Future Climate Scenarios

We used a simple, but very effective, statistical downscaling method based on the Delta method (Fowler et al. 2007), which has been successfully applied to Ecuadorian landscapes before (Buytaert et al. 2009). The Delta method provides future scenarios for precipitation and temperature. The latter was also used to calculate potential evapotranspiration using the Penman–Monteith approach. For the input variables wind speed and radiation, the values for 2007/2008 were used. The Delta method utilizes differences between the current and future GCM simulations. The anomalies between the average value of each variable of the modeled historical time slice (1960–1990) and the future time slice are then applied to given observations for 2007/2008 by simple scaling. This method has the shortcoming that variability remains static and spatial patterns are not considered. However, it has its advantages in cases where only a limited amount of data is available as it is the case in our study. Additionally, the local climate system of the southern Andes is highly complex, preventing the application of more sophisticated downscaling methods.

Projections for precipitation and maximum and minimum temperature were generated for three time slices (2010–2039, 2040–2069, 2070–2099) and two emission scenarios (A1B and A2) from IPCC Assessment Report 4 from eight GCMs (BCM2, CSMK3.0, CSMK3.5, GFCM20, GFCM2.1, INCM3, MIMR, NCCCSM3). GCM data were obtained from http://www.ipcc-data.org. The generated time series for the three time slices reflect a representative time series during that period; they are not meant to be predictions for a particular year within each time slice.

19.2.2 Hydrological Modeling

With regard to the already observed structural model uncertainty to predict rainfall-runoff reaction in tropical mountainous catchments (Plesca et al. 2012), we applied a set of seven hydrological models to predict the likely impacts of climate change on hydrology in tropical montane rainforests of southern Ecuador. The complexity of the participating models ranges from the most simple, lumped (HBV-light, LASCAM, CHIMP, HEC-HMS, NAM) to more distributed (HBV-N-D) and more process-oriented models (SWAT). The major differences between the models

are the spatial representation (regular pixels, semi-lumped subcatchments, or fully lumped concepts representation) and the type of infiltration processes used by the models. For a more detailed model description the reader is referred to Plesca et al. (2012). In addition, we also included the NAM model in our study. NAM is a conceptual lumped rainfall-runoff model, simulating the flow by its water balance components. NAM's performance showed a Nash–Sutcliffe efficiency of 0.59 and 0.52 as well as a log-biased constrained efficiency of 0.50 and 0.44 during calibration and validation, respectively (Plesca et al. 2012).

In order to simulate the climate change impact on the hydrological regimes of the river San Francisco, we ran the models under the A1B and A2 scenarios and the seven GCMs, following the hypothesis that the application of an ensemble of models generally increases the credibility of prediction (Tebaldi et al. 2010). To reduce the heterogeneity of model forcing data we applied the same input data and the same spatial interpolation procedures for precipitation and temperature (the inverse distance weighted method). In this sense we also developed a common potential evapotranspiration dataset used by all models to focus on the different structures in rainfall-runoff generation rather than on any other potentially effective model input data.

Since measured discharge data are available for only 14 months, all models have been calibrated to the first 10 months and were validated for the 4 remaining months (Fig. 19.2). We used a 12 months spin up time for all models by simply copying the available time series as a pre-run time period.

We consider the output of mean monthly average runoff as well as the maximum, minimum, and mean discharge from the seven hydrological models as a combined information for this model ensemble and observations to determine the response of runoff under the A1B and A2 scenarios.

19.3 Results and Discussion

19.3.1 Effects on Local Climate

The results of the downscaling method are displayed in Fig. 19.3. To illustrate the predicted local climate change impact for the three periods 2010–2039, 2040–2069, and 2070–2099 of the IPCC scenarios A1B and A2, simulated data are compared to measured data from the ECSF climate station for a 14-month period in 2007–2008. Results for both emission scenarios A1B and A2 revealed similar dynamics. However, increases in precipitation are substantially higher for A2. For the sake of clarity, the presented results focus on the A1B scenario.

The monthly means of temperature show a clear increase over the three periods. Until 2070–2099, the annual average temperature is expected to rise by about 2.9 °C. It is worth to note that the biggest monthly differences of the mean temperatures occur in June and March, with temperature increases of 3.4 °C and

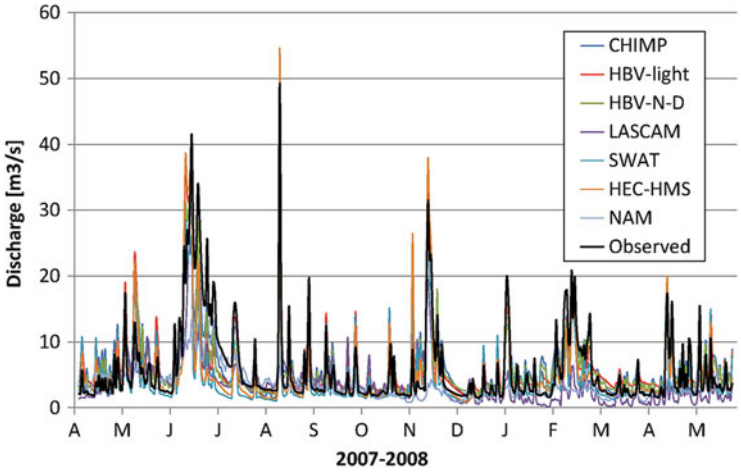

Fig. 19.2 Simulated discharge [$m^3\ s^{-1}$] for the reanalyzed (RA) period: 2000–2009. The *black curve* shows the observed discharge for a period of 14 months. For more information about each model simulation results, see Plesca et al. (2012). See text for further information about the applied models

3.5 °C, respectively. The change of the minimum and maximum temperature is nearly equivalent to the mean temperature and shows a steady upward trend. Annual mean minimum temperature increases from 11.2 °C in the reference period to 14.2 °C in the period 2070–2099, and the annual mean maximum temperature rises from 20.7 °C to 23.4 °C, respectively. The lines of minimum and maximum temperatures indicate the lower and upper bounds of predicted changes from the eight GCMs used in this study.

Boxplots in Fig. 19.3 depict the changes in monthly precipitation. Each boxplot shows the range of the calculated monthly mean precipitation of the applied GCMs. It is noteworthy that boxplots for May and June exhibit a considerably greater dispersion than boxplots for the other months (average standard deviation 25 mm) with 157 mm and 300 mm, respectively.

The annual rainfall from April 2007 until March 2008 amounted to 1.873 mm. For the three simulated time periods, annual rainfall increases up to 2.395 mm. Until the first future period (2010–2039), rainfall raises by about 11 %, approximately by additional 4 % in the second period and in 2070–2099 by further 10 %, compared to the previous time period. Mainly affected are months with extreme precipitation, i.e., May and June for which the amount of rainfall is expected to double in comparison to the reference period. This strong increase goes along with a general decreasing trend in precipitation from September to November. As in the reference period, the increase in precipitation in May and June is accompanied by a strong decrease in the maximum and an increase in the minimum temperature.

In general, the calculated time series for the climate change scenarios follow the typical precipitation regime of the reference period. Of course, this is due to the simple approach of downscaling that does not consider changes in variability or extremes. The peak in May and June becomes much more distinct in the future

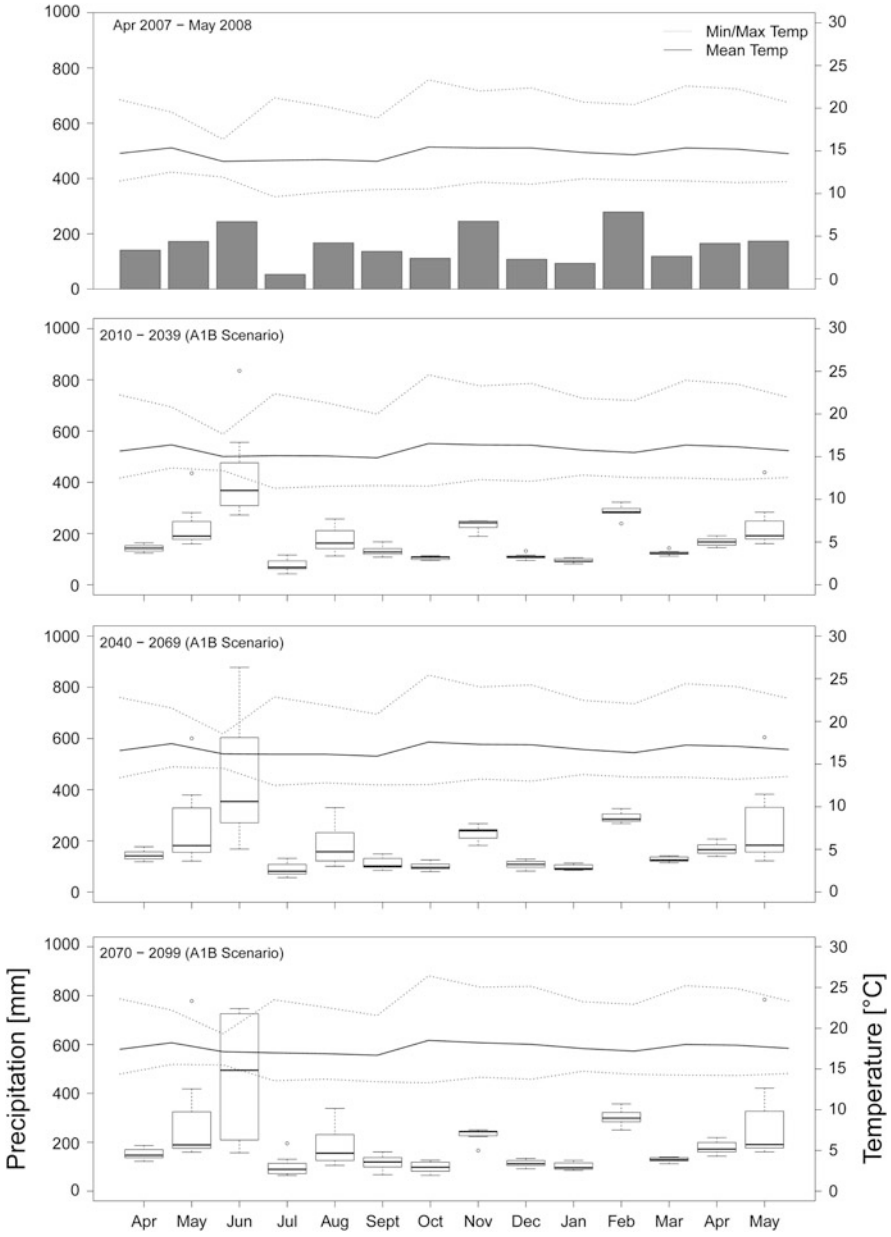

Fig. 19.3 Measured and predicted temperature (*lines*) and precipitation (*bars*) for the climate station ECSF. Reference period is April 2007–May 2008 and predictions are 2010–2039, 2040–2069, and 2070–2099 for the IPCC emission scenario A1B. Predictions represent the same 14-month time series under climate change impact (see details in text for the method applied). *Dotted lines* show minimum and maximum temperatures calculated by the eight downscaled GCMs. *Boxplots* represent results of predicted precipitation by the same ensemble

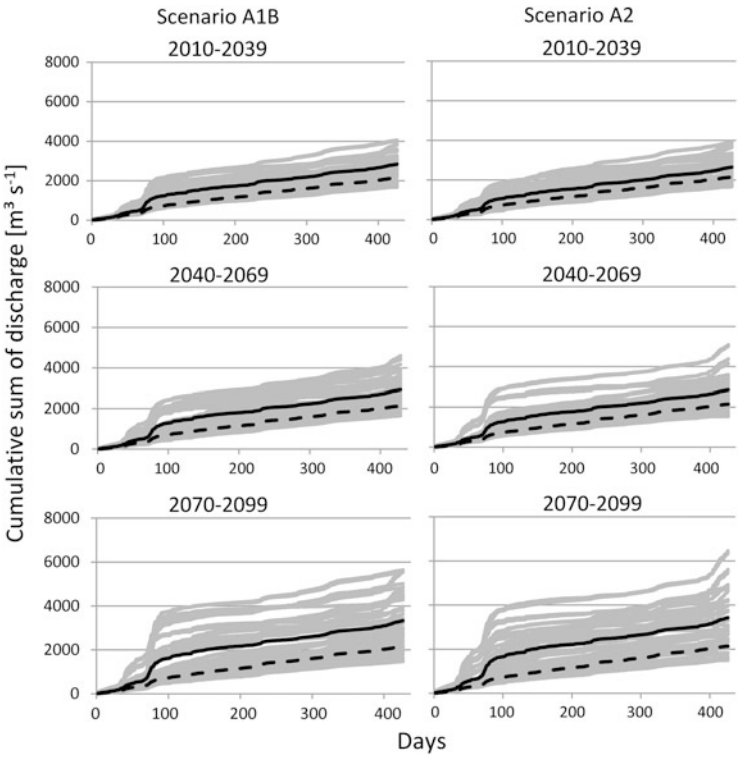

Fig. 19.4 Average discharge (*solid black line*) based on seven hydrological models and eight GCM realization for the A1B (*left*) and A2 (*right*) emission scenarios. Single model forecasts ($n = 56$) are represented by the cohort of *gray lines*. Observed discharge under current conditions is shown as *dashed black line*

simulations, and in the already dryer period (from September to November), rainfall decreases slightly by 10 % on average.

One has to keep in mind that the anomalies of the climate change scenarios were derived by utilizing the time series from 1960 to 1990 as a reference. However, we assume that this period is comparable to the available observed time series 2007–2008 and that basically no changes occurred between the two time slices which is probably untrue. Ideally, the anomalies should be calculated with reference to a matching 30-year period that encompasses the observed period. Unfortunately, such data are not available for the ECSF station.

19.3.2 Effects on Local Hydrology

Both emission scenarios A1B and A2 lead to similar predictions with regard to discharge dynamics. Figure 19.4 shows the cumulative sum of daily discharge for the simulation period of 14 months for all models ($n = 7$) and all downscaled

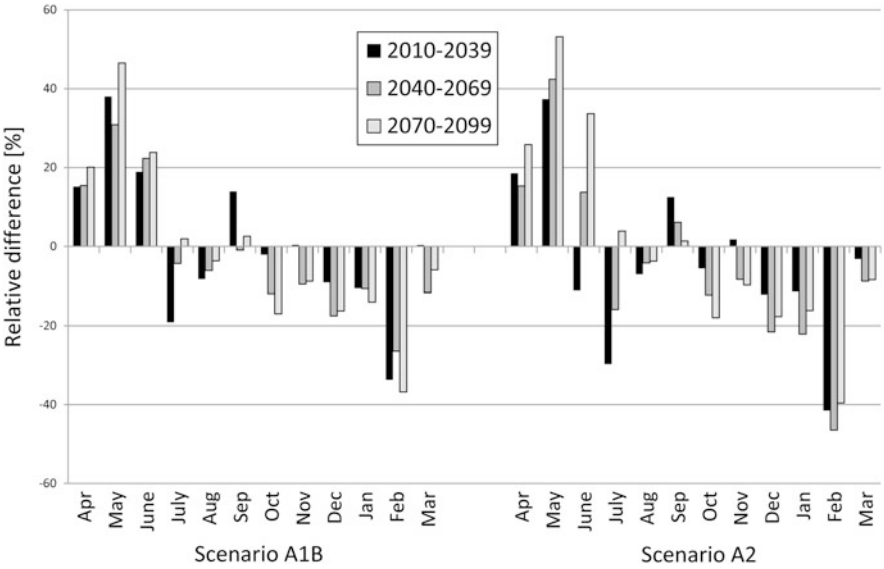

Fig. 19.5 Relative differences [%] between mean monthly observed discharge in 2007–2008 and the projected time slices 2010–2039, 2040–2069, and 2070–2099 for emission scenarios A1B (*left*) and A2 (*right*)

GCMs ($n = 8$). Mean discharge is calculated based on the cohort of all model runs ($n = 56$). For the first time slice 2010–2039 forecasts for both emission scenarios are well in agreement with respect to both the mean of all forecasts and the behavior of single model runs. As can be seen in comparison to the cumulative discharge of the current situation (2007–2008) total discharge is substantially increasing by around 35–40 %. The overall pattern of single model forecasts is somehow changing for the following time slice, where despite similar mean predictions of the model ensemble a larger deviation between single model runs can be depicted. This trend is even further amplified in the last time slice 2070–2099 where more and more models tend to predict larger discharge volumes for the A2 emission scenario, especially towards the end of the simulation period. In comparison to the observed discharge under current conditions, increases are forecasted to around 80 %.

In order to find out which periods of the year have the highest impacts on discharge under current and future climate conditions, we analyzed the relative differences between mean monthly discharge for the observation period 2007–2008 and the predictions of the hydrological models (Fig. 19.5). Similar results were found for both scenarios in the case of relative differences. Monthly discharges for April, May, and June expect an increase in the order of 13–53 %, which is compensated by reduced discharge from October to February (Fig. 19.5). On average, following the A1B scenario, mean discharges are predicted to increase by 0.3 % for 2010–2039, whilst for 2040–2069 and 2070–2099 reduced discharge of −2.55 and −0.63 % are expected, respectively. While the general pattern of

Table 19.1 Expected impact of future climate trends on water-related ecosystem services in the San Francisco River valley (definitions in agreement with the Millennium Ecosystem Assessment 2005; see also Chap. 9)

	Climate change impact	Note
Provisioning service: fresh water	↑	Hydropower generation can expect increasing benefits due to increasing amount of available water
Regulating service: water purification and waste treatment	→	Water quality will remain stable at high-quality levels with sufficient amount of water available for dilution
Regulating service: water regulation	↓	Increasing amounts of discharge and number of extreme precipitation events especially in May and June are likely to increasing flood occurrences and potentially erosion events. However, due to low local population number, the economic losses are expected to be of minor value; this might be different in downstream catchments with larger population

Climate change increases provisioning services, if human consumption of the service is likely to increase. An increase for regulating service is predicted, if climate change improves the service from the human perspective. Supporting services are not directly used and climate change impacts the supply of all other services. If these indirect effects are listed, supporting service would be double counted. ↑ increasing/enhancing, → no change, ↓ decreasing

changes in discharge is similar for the emission scenario A2, absolute changes are somewhat more pronounced. This is, in fact, contrasting with the general increase in precipitation shown in Fig. 19.3. Increasing temperatures and resulting larger losses through evapotranspiration (data not shown) may be a reason for this seaming discrepancy. It has to be noted that other parameters like wind speed, relative humidity, or global radiation that strongly influence evapotranspiration were also not altered during the simulations as no GCM projections were available. Especially global radiation might severely affect the estimation of evapotranspiration as it is usually the most sensitive parameter in the Penman–Monteith equation. Increasing cloud cover in the future might reduce incoming global radiation and thus have a negative feedback on evapotranspiration rates.

19.4 Conclusion: Impact of Climate Change on Water-Related Ecosystem Services in the Future

Based on the results obtained in the hydrological scenarios considering climate change impact, we conclude that most water-related ecosystem services are only affected to a minor degree, as summarized in Table 19.1. The largest change among all is expected for provisioning services. Here increasing water volumes can be

directly used to increase hydropower generation. Water quality will remain on a very high level, as nutrients are effectively retained in the ecosystem and subsequent losses are small. But even if nutrients are lost, they are diluted due to the availability of large water volumes. Increasing precipitation might trigger flood events and landslide occurrences, effecting regulating services. From an anthropogenic viewpoint, economic losses will remain low in the research area due to the low density of population and infrastructure.

References

Bendix J, Behling H, Peters T, Richter M, Beck E (2010) Functional biodiversity and climate change along an altitudinal gradient in a tropical mountain rainforest. In: Tscharnke T, Leuschner C, Veldkamp E, Faust H, Guhardja E, Bidin A (eds) Tropical rainforests and agroforests under global change. Springer, Heidelberg, pp 239–268

Buytaert W, Celleri R, Time L (2009) Predicting climate change impacts on water resources in the tropical Andes: effects of GCM uncertainty. Geophys Res Lett 36, L07406. doi:10.1029/2008GL037048

Fowler HJ, Blenkinsop S, Tebaldi C (2007) Linking climate change modelling to impacts studies: recent advances in downscaling techniques for hydrological modelling. Int J Climatol 27:1547–1578

Millennium Ecosystem Assessment (2005) Ecosystems and human well-being: synthesis. Island Press, Washington, DC

Plesca I, Timbe E, Exbrayat J-F, Windhorst D, Kraft P, Crespo P, Vaché KB, Frede H-G, Breuer L (2012) Model intercomparison to explore catchment functioning: results from a remote montane tropical rainforest. Ecol Model 239:3–13. doi:10.1016/j.ecolmodel.2011.05.005

Tebaldi C, Smith RL, Nychka D, Mearns LO (2010) Quantifying uncertainty in projections of regional climate change: a Bayesian approach to the analysis of multimodel ensembles. J Climate 18:1524–1540

Urrutia R, Vuille M (2009) Climate change projections for the tropical Andes using a regional climate model: temperature and precipitation simulations for the end of the 21st century. J Geophys Res 114, D02108. doi:10.1029/2008JD011021